materials

MDPI

Article

High Optical Response of Niobium-Doped WSe_2-Layered Crystals

Hung-Pin Hsu [1], Der-Yuh Lin [2,*], Jhin-Jhong Jheng [2], Pin-Cheng Lin [2] and Tsung-Shine Ko [2]

[1] Department of Electronic Engineering, Ming Chi University of Technology, New Taipei City 24301, Taiwan; hphsu@mail.mcut.edu.tw

[2] Department of Electronic Engineering, National Changhua University of Education, Changhua 50074, Taiwan; M0453002@mail.ncue.edu.tw (J.-J.J.); M0653013@mail.ncue.edu.tw (P.-C.L.); tsko@cc.ncue.edu.tw (T.-S.K.)

* Correspondence: dylin@cc.ncue.edu.tw; Tel.: +886-4-7232105 (ext. 8357)

Received: 24 January 2019; Accepted: 9 April 2019; Published: 10 April 2019

Abstract: The optical properties of WSe_2-layered crystals doped with 0.5% niobium (Nb) grown by the chemical vapor transport method were characterized by piezoreflectance (PzR), photoconductivity (PC) spectroscopy, frequency-dependent photocurrent, and time-resolved photoresponse. With the incorporation of 0.5% Nb, the WSe_2 crystal showed slight blue shifts in the near band edge excitonic transitions and exhibited strongly enhanced photoresponsivity. Frequency-dependent photocurrent and time-resolved photoresponse were measured to explore the kinetic decay processes of carriers. Our results show the potential application of layered crystals for photodetection devices based on Nb-doped WSe_2-layered crystals.

Keywords: 2D chalcogenides; photoconductivity; photoresponse

1. Introduction

Two-dimensional (2-D) semiconductors have attracted much attention since the discovery of graphene. Two-dimensional transition metal dichalcogenides (TMDCs) MX_2 (M = transition metal; X = chalcogen) have shown their potential for optoelectronic and nanoelectronic applications [1–5]. Compared to graphene, layered TMDCs exhibit semiconductor, metallic and semi-metallic behaviors [6–8]. The bandgap properties can be changed from indirect to direct by varying the number of layers [9,10]. Other novel physical properties, such as spin-orbit band splitting and valleytronics [11–14], have been investigated as well. Top-gated transistors and high gain phototransistors based on the MoS_2-layered semiconductor were also successfully developed [15,16]. MoS_2 is well known to be a native n-type semiconductor, and p-doped MoS_2 has also been achieved via intentional doping [17,18]. However, both n- and p-type semiconductors are needed for complementary digital logic electronic devices [19]. P-type behaviors have been observed in bulk and mechanically exfoliated monolayer and few-layer WSe_2 [20]. Recently, theoretical and experimental studies reported modifications to optical [21,22], magnetic [23–25], and catalytic [26] properties induced by doping into TMDCs. The carrier type in layered TMDCs can also be modified by metal work-function engineering [27,28], electrostatic doping [29,30], surface functionalization [31,32], or charge transfer from physi-sorbed volatile molecules [33]. However, the replacement of the host atom with dopant is required because the covalent bonding inside the lattice is more stable in practical optoelectronics devices. Previously, it has been demonstrated that a certain amount of Nb (~0.5%) doping will generate acceptor states in MoS_2, making the conduction type change from n-type to p-type [18]. However, few studies have been done on the use of Nb as a dopant in TMDCs such as WS_2 (~0.55%) [34] or WSe_2 (~0.17%) [35]. Impurity doping will create defect states that might change the carrier transport

properties in 2-D materials. Hence, further exploration of the doping effects of 2-D TMDCs should be carried out.

A previous study revealed the enhanced photoresponsivity with Nb (~0.17%) doped into WSe_2 [35]. It would be interesting to investigate the optical properties with the use of a higher Nb content in WSe_2. Usually, high concentration doping is difficult to achieve in the initial stage. Hence, we chose a doping concentration of Nb of up to ~0.5%, which is similar to that used in other reported studies [18,34], and investigated the optical characteristics. In this work, we report the optical investigations of Nb-doped WSe_2-layered crystals by piezoreflectance (PzR), photoconductivity (PC), spectroscopy, frequency-dependent photocurrent, and time-resolved photoresponse. The near band edge excitonic transitions were probed by PzR and PC spectra. The optical response was also carried out by frequency-dependent photocurrent and time-resolved photoresponse. We will report the optical measurements and discuss the possible mechanisms in this study.

2. Materials and Methods

The Nb-doped tungsten diselenide (WSe_2) layered crystals were grown from 4N mixed elements (W: 99.99%; Se: 99.99%; and Nb: 99.99%) by the chemical-vapor transport (CVT) method. Chemical transport was achieved with ICl_3 as the transport agent in an amount of about 0.3 g. The weight of the doping material was determined stoichiometrically to obtain a concentration of 0.5% Nb. The total charge used in the growth experiment was about 5 g. Prior to the crystal growth, the powdered compounds of the series were prepared from the elements through a reaction at 950 °C for 2 days in evacuated quartz ampoules. After cooling down to room temperature, the mixture was transferred into a three-zone furnace and slowly heated to 950 °C. In order to avoid any explosions due to strongly exothermic reactions between the mixed elements, slow heating was necessary. The growth temperature was about 850 °C with a temperature gradient of about 3 °C/cm and a growth time of ~15 days. Single crystals with layered structure were formed in silver-colored platelets with a thickness of ~20 um and lateral size of 2 mm × 3 mm.

For PzR measurements, the samples were glued on a 0.15 cm thick lead–zirconate–titanate (PZT) piezoelectric transducer driven by an 800 V_{rms} sinusoidal wave at ~200 Hz. The alternating expansion and contraction of the transducer subjected the sample to an alternating strain with a typical rms $\Delta l/l$ value of ~10^{-5}. A 150 W tungsten-halogen lamp filtered by a PTI 0.25 m monochromator provided the incident monochromatic light. The reflected light was detected by a silicon photodetector (EG&G HUV-2000B, MD, USA). The dc output of the photodetector was maintained at a constant level throughout the experiment by an electronic servo mechanism with a variable neutral density filter. A dual-phase lock-in amplifier (Perkin-Elmer 7265, MA, USA) was used to measure the detected signals. For PC measurements, the spectra were measured as a function of the photon energy in the range from 1.0 to 2.3 eV by the probe beam with several μW, and the probe beam was chopped at ~10 Hz. For frequency-dependent photocurrent measurement, a voltage (5 V) was supplied by the source meter (Keithley 2400, OH, USA), and a 652 nm laser (~2 mW) was used as the excitation illumination. The dc photocurrent represented the steady state photocurrent at 0 Hz. Afterwards, an ac photocurrent was induced in the frequency range from 0.5 to 10 kHz. The time-resolved photoresponse signals were collected by a data acquisition (DAQ) device with time resolution of 1 μs.

3. Results and Discussion

Figure 1 shows the PzR spectra of undoped and 0.5% Nb-doped WSe_2-layered crystals in the range from 1.3 to 2.35 eV at room temperature. As shown in the figure, two prominent near band edge excitonic transitions, A and B, of undoped and 0.5% Nb-doped WSe_2 can be clearly observed. In order to determine the excitonic transitions from PzR spectra, we fit the experimental spectra with a theoretical line shape. The solid curves are the least-square fits to the first derivative Lorentzian line shape function [36,37]:

$$\frac{\Delta R}{R} = \mathrm{Re}\sum_{j=1} A_j e^{i\Phi_j}(E - E_j + i\Gamma_j)^{-n} \quad (1)$$

where A_j and Φ_j are the amplitude and phase of the line shape, E_j and Γ_j are the energy and broadening parameter of the excitonic transitions, and the value of n depends on the origin of the transitions. For the derivative functional form, n = 2 is appropriate for the bound states, such as excitons. The determined near band edge excitonic transitions of E_j are denoted as A and B and are indicated by arrows in Figure 1. The obtained values of near band edge excitonic transitions A and B were 1.620 and 2.083 eV for undoped WSe_2, whereas the excitonic transitions shifted to slightly higher energy levels with A and B showing values of 1.632 and 2.102 eV in Nb-doped WSe_2 crystals. The PzR spectra revealed excitonic transitions with a slightly blue-shift following niobium incorporation. This blue-shift excitonic transition behavior was also observed in Nb-doped MoS_2 by reflectance difference spectra [38]. The blue-shifted excitonic transitions in the present work might be due to the Burstein–Moss shift in the Nb-doped WSe_2. Figure 2 shows the PC spectra for undoped and 0.5% Nb-doped WSe_2-layered crystals. As shown in PC, we can observe that the WSe_2 indirect band gap rose from ~1.2 eV. The other two features around 1.6 and 2.1 eV were attributed to the A and B excitonic transitions, respectively. It is shown that both the indirect band gap and direct excitonic transition can be measured by PC; however, the direct excitonic transition can be probed by PzR spectra with better accuracy for the determination of transition positions due to its derivative nature [39]. As compared with the undoped WSe_2 sample, the photoresponsivity with Nb = 0.17% was enhanced by a factor of 10 [35]. However, the sample with Nb = 0.5% exhibited a much higher photoresponsivity intensity (~400 times) than the undoped one. In this study, the photoresponsivity can be increased significantly by incorporation of only a tiny amount of Nb (~0.5%) The value of undoped WSe_2 (several mA/W) in this study is smaller than the value of few-layered WSe_2 reported by Wang et al. (~600 mA/W) [40]. This result might be due to defects, which results in an inferior crystal quality and causes lower photoresponsivity in the PC measurement. However, the value of enhanced photoresponsivity in Nb =0.5 % WSe_2 was ~3.5 A/W, which is comparable with previous studies based on multi-layered or mono-layer MoS_2 photodetection devices [41,42]. The obtained photoresponsivity values for the Nb-doped WSe_2 from this work and the MoS_2 based photodetection devices from previous reports [40–42] are listed in Table 1.

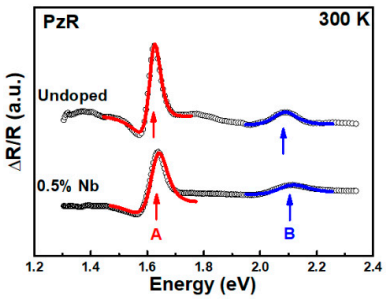

Figure 1. Experimental piezoreflectance (PzR) spectra of undoped and 0.5% Nb-doped WSe_2-layered crystals at 300 K. The solid curves are the fits to the first derivative Lorentzian line shape. The obtained near band edge excitonic transitions A and B are indicated by arrows.

Table 1. Comparison of photoresponsivity for the WSe_2 and MoS_2 based photodetection devices.

Structure	Thickness	Photoresponsivity	Ref.
WSe_2 (undoped)	bulk	8 mAW^{-1}	this work
WSe_2 (0.5% Nb)	bulk	3.5 AW^{-1}	this work
WSe_2 phototransistor	few-layers	600 mAW^{-1}	[40]
MoS_2/Si heterojunction	multi-layers	8.75 AW^{-1}	[41]
MoS_2 phototransistor	mono-layer	1 AW^{-1}	[42]

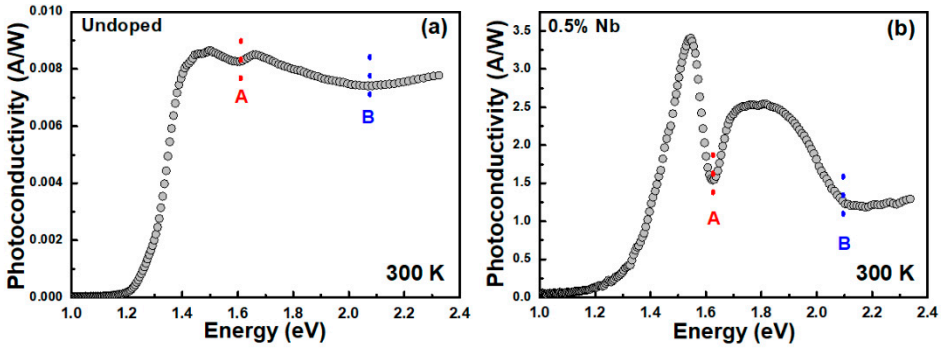

Figure 2. The photoconductivity (PC) spectra of (**a**) undoped and (**b**) 0.5% Nb-doped WSe_2-layered crystals at 300 K. The excitonic transitions A and B are indicated by arrows.

In order to understand the frequency response properties of undoped and 0.5% Nb-doped WSe_2-layered crystals for the application in optoelectronic devices, the frequency-dependent photocurrent was also measured. To understand the carrier kinetics from the photoconductivity measurement, the frequency dependence of the photocurrent I_{ac}/I_{dc} was measured, where I_{ac} is the ac component of the photocurrent and I_{dc} represents the steady state photocurrent. A light illumination source of 652 nm laser was used. Figure 3 illustrates the frequency-dependent photocurrent as a function of frequency for undoped and 0.5% Nb-doped layered crystals. It can be observed that the I_{ac}/I_{dc} of Nb-doped crystal decreased faster than that of the undoped one as the frequency increased. The behavior of the frequency-dependent photocurrent can be described by the relation [43]

$$I_{ac}/I_{dc} = k_1 \times \tanh\left(\frac{1}{4f\tau_1}\right) + k_2 \times \tanh\left(\frac{1}{4f\tau_2}\right) \quad (2)$$

where K_1 and K_2 are the amplitude coefficients. τ_1 and τ_2 are the carrier time constants of long and short time decay processes. The obtained values of the coefficients are listed in Table 2. In the frequency range from 0.5 to 10 kHz, the photocurrent decay in the Nb-doped crystal was composed of 67% long time and 33% short time processes. Compared to undoped WSe_2 crystal, the proportion of long time constant decay process in Nb-doped crystal was larger than short time constant decay process. This might be attributed to additional trap states generated from the incorporation of niobium, which cause the longer decay process.

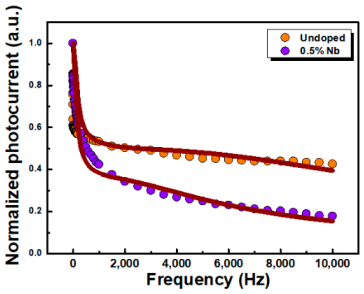

Figure 3. Normalized photoconductivity as a function of the frequency of undoped and 0.5% Nb-doped WSe_2-layered crystals.

Table 2. The obtained values of coefficients from the least-square fits to Equation (2) for undoped and 0.5% Nb-doped WSe_2-layered crystals.

Specimen	K_1	τ_1 (ms)	K_2	τ_2 (μs)
WSe_2 (undoped)	0.52	2.5	0.48	22
WSe_2 (0.5% Nb)	0.67	3.1	0.33	51

To study the time-resolved photoresponse dynamics of undoped and Nb-doped WSe_2-layered crystals, we applied ON/OFF light modulation at an incident light of 500 Hz and measured the rise and fall time constants. The time-resolved photoresponses of undoped and 0.5% Nb-doped layered crystals were further investigated and are shown in Figure 4a,b. The magnified and normalized plots of one response cycle are shown in Figure 4c,d. The speed response is characterized by the rise time (τ_r) and the fall time (τ_f). The rise time and fall time are defined as the time interval for the response rise from 10% to 90%, and the decay from 90% to 10% of the maximum photocurrent value, respectively [44]. The rise and fall time for undoped WSe_2 was 42 µs. Further analysis of the 0.5% Nb-doped WSe_2 revealed a larger rise time of 150 µs, as well as a larger fall time of 612 µs, which represents the slower photo response speed of Nb-doped crystal. It is noticed here that the timescales in the time-resolved photoresponse are different with the time constant determined by frequency-dependent photocurrent. This is because the rise and fall time originate from the combined contribution of both long and short time processes. This phenomenon is more pronounced with the incorporation of niobium which results in the rise and fall values being between long- and short-time constants. For the undoped WSe_2, the response time is comparable with the previously reported TMDC values [45,46]. Nevertheless, the slower time response in Nb-doped crystal might be due to the influence of trap states induced by niobium impurity doping. The trap states could deteriorate the carriers' transfer speed in the doped crystal [43]. The slower response speed that arises from trap states could also correlate with the enhanced photoresponsivity in PC measurement. The trap level produced by the doping atoms traps photoexcited carriers; then, the carriers could hop from trap level to energy band, continuously contributing to the photocurrent. For the sample with a Nb content of only 0.17%, the increased photoresponsivity was not as pronounced as in the sample with Nb = 0.5%. However, this mechanism makes the rise and fall response time longer in time-resolved measurement. The enhanced photoresponsivity accompany with slower time response in the Nb = 0.5%-doped sample provide a trade-off reference for optimizing the design of high performance photodetectors. The doping of niobium atoms creates trap states close to the energy band, which causes the enhancement of photoresponsivity as well as slowing down the response speed.

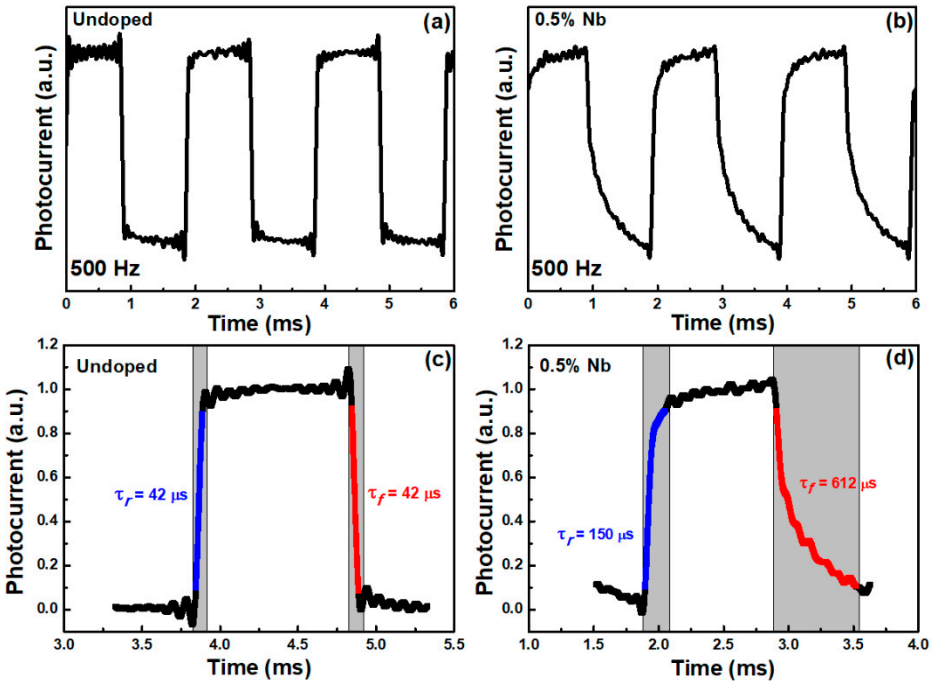

Figure 4. Time-resolved photoresponse of (**a**) undoped and (**b**) 0.5% Nb-doped WSe_2-layered crystals at 500 Hz. The enlarged and normalized plots of (**c**) undoped and (**d**) 0.5% Nb-doped WSe_2-layered crystals of one response cycle for calculating the rise and fall times.

4. Conclusions

In conclusion, we studied optical properties, PzR, PC, frequency-dependent photocurrent, and time-resolved photoresponse, of 0.5% Nb-doped WSe_2-layered crystals grown by the chemical vapor transport method. The near band edge excitonic transitions A and B were observed by PzR and PC spectra and showed a slight blue-shift of excitonic transitions following niobium incorporation. From the PC results, we found enhanced light illumination responsivity with the incorporation of Nb. The frequency dependence photocurrent results indicate that there is a larger portion of long decay processes in Nb-doped crystal. The time-resolved photoresponse analysis showed that the response time of Nb-doped crystal is larger than that of undoped crystal. Both the frequency dependence photocurrent and the time-resolved photoresponse investigation revealed lower response dynamics with the doping process, which was attributed to the additional trap states that result from the presence of niobium atoms. These results could be helpful for the optimization of photodetection applications based on TMDC-layered semiconductors.

Author Contributions: Conceptualization, H.-P.H. and D.-Y.L.; methodology, D.-Y.L. and T.-S.K.; formal analysis, H.-P.H. and D.-Y.L.; investigation, J.-J.J. and P.-C.L.; resources, D.-Y.L. and T.-S.K.; data curation, J.-J.J. and P.-C.L.; writing—original draft preparation, H.-P.H. and D.-Y.L.; writing—review and editing, H.-P.H. and D.-Y.L.

Funding: This research was funded by Ministry of Science and Technology (MOST 107-2221-E-131-032 and MOST 107-2112-M-018-002).

Conflicts of Interest: The authors declare no conflict of interest.

References

1. Wang, Q.H.; Kalantar-Zadeh, K.; Kis, A.; Coleman, J.N.; Strano, M.S. Electronics and optoelectronics of two-dimensional transition metal dichalcogenides. *Nat. Nanotech.* **2012**, *7*, 699–712. [CrossRef]
2. Mak, K.F.; He, K.; Lee, C.; Lee, G.H.; Hone, J.; Heinz, T.F.; Shan, J. Tightly bound trions in monolayer MoS_2. *Nat. Mater.* **2013**, *12*, 207–211. [CrossRef]
3. Mak, K.F.; Shan, J. Photonics and optoelectronics of 2D semiconductor transition metal dichalcogenides. *Nat. Photon.* **2016**, *10*, 216–226. [CrossRef]
4. Amani, M.; Lien, D.H.; Kiriya, D.; Xiao, J.; Azcatl, A.; Noh, J.; Madhvapathy, S.R.; Addou, R.; KC, S.; Dubey, M.; et al. Near-unity photoluminescence quantum yield in MoS_2. *Science* **2015**, *350*, 1065–1068. [CrossRef] [PubMed]
5. Li, M.Y.; Shi, Y.; Cheng, C.C.; Lu, L.S.; Lin, Y.C.; Tang, H.L.; Tsai, M.L.; Chu, C.W.; Wei, K.H.; He, J.H.; et al. Epitaxial growth of a monolayer WSe_2-MoS_2 lateral p-n junction with an atomically sharp interface. *Science* **2015**, *349*, 524–528. [CrossRef] [PubMed]
6. Ganatra, R.; Zhang, Q. Few-Layer MoS_2: A promising layered semiconductor. *ACS Nano* **2014**, *8*, 4074–4099. [CrossRef]
7. Lin, Y.C.; Dumcenco, D.O.; Huang, Y.S.; Suenaga, K. Atomic mechanism of the semiconducting-to-metallic phase transition in single-layered MoS_2. *Nat. Nanotech.* **2014**, *9*, 391–396. [CrossRef] [PubMed]
8. Cho, S.; Kim, S.; Kim, J.H.; Zhao, J.; Seok, J.; Keum, D.H.; Baik, J.; Choe, D.H.; Chang, K.J.; Suenaga, K.; et al. Phase patterning for ohmic homojunction contact in $MoTe_2$. *Science* **2015**, *349*, 625–628. [CrossRef]
9. Lee, C.; Yan, H.; Brus, L.E.; Heinz, T.F.; Hone, J.; Ryu, S. Anomalous lattice vibrations of single- and few-layer MoS_2. *ACS Nano* **2010**, *4*, 2695–2700. [CrossRef]
10. Mak, K.F.; Lee, C.; Hone, J.; Shan, J.; Heinz, T.F. Atomically thin MoS_2: A new direct-gap semiconductor. *Phys. Rev. Lett.* **2010**, *105*, 136805. [CrossRef]
11. Yuan, H.; Wang, X.; Lian, B.; Zhang, H.; Fang, X.; Shen, B.; Xu, G.; Xu, Y.; Zhang, S.C.; Hwang, H.Y.; et al. Generation and electric control of spin-valley-coupled circular photogalvanic current in WSe_2. *Nat. Nanotech.* **2014**, *9*, 851–857. [CrossRef]
12. Xiao, D.; Liu, G.B.; Feng, W.; Xu, X.; Yao, W. Coupled spin and valley physics in monolayers of MoS_2 and other group-VI dichalcogenides. *Phys. Rev. Lett.* **2012**, *108*, 196802. [CrossRef]
13. Zeng, H.; Dai, J.; Yao, W.; Xiao, D.; Cui, X. Valley polarization in MoS_2 monolayers by optical pumping. *Nat. Nanotech.* **2012**, *7*, 490–493. [CrossRef]

14. Mak, K.F.; He, K.; Shan, J.; Heinz, T.F. Control of valley polarization in monolayer MoS_2 by optical helicity. *Nat. Nanotech.* **2012**, *7*, 494–498. [CrossRef]
15. Zhang, W.; Huang, J.K.; Chen, C.H.; Chang, Y.H.; Cheng, Y.J.; Li, L.J. High-gain phototransistors based on a CVD MoS_2 monolayer. *Adv. Mater.* **2013**, *25*, 3456–3461. [CrossRef]
16. Radisavljevic, B.; Radenovic, A.; Brivio, J.; Giacometti, V.; Kis, A. Single-layer MoS_2 transistors. *Nat. Nanotech.* **2011**, *6*, 147–150. [CrossRef]
17. Chen, M.; Nam, H.; Wi, S.; Ji, L.; Ren, X.; Bian, L.; Lu, S.; Liang, X. Stable few-layer MoS_2 rectifying diodes formed by plasma-assisted doping. *Appl. Phys. Lett.* **2013**, *103*, 142110. [CrossRef]
18. Suh, J.; Park, T.E.; Lin, D.Y.; Fu, D.; Park, J.; Jung, H.J.; Chen, Y.; Ko, C.; Jang, C.; Sun, Y.; et al. Doping against the native propensity of MoS_2: Degenerate hole doping by cation substitution. *Nano Lett.* **2014**, *14*, 6976–6982. [CrossRef]
19. Huang, J.K.; Pu, J.; Hsu, C.L.; Chiu, M.H.; Juang, Z.Y.; Chang, Y.H.; Chang, W.H.; Iwasa, Y.; Takenobu, T.; Li, L.J. Large-area synthesis of highly crystalline WSe_2 monolayers and device applications. *ACS Nano* **2014**, *8*, 923–930. [CrossRef]
20. Fang, H.; Chuang, S.; Chang, T.C.; Takei, K.; Takahashi, T.; Javey, A. High-performance single layered WSe_2 p-FETs with chemically doped contacts. *Nano Lett.* **2012**, *12*, 3788–3792. [CrossRef]
21. Xu, E.Z.; Liu, H.M.; Park, K.; Li, Z.; Losovyj, Y.; Starr, M.; Werbianskyj, M.; Fertig, H.A.; Zhang, S.X. p-Type transition-metal doping of large-area MoS_2 thin films grown by chemical vapor deposition. *Nanoscale* **2017**, *9*, 3576–3584. [CrossRef]
22. Kong, L.J.; Liu, G.H.; Qiang, L. Electronic and optical properties of O-doped monolayer MoS_2. *Comput. Mater. Sci.* **2016**, *111*, 416–423. [CrossRef]
23. Zhao, P.; Zheng, J.; Guo, P.; Jiang, Z.; Cao, L.; Wan, Y. Electronic and magnetic properties of Re-doped single-layer MoS_2: A DFT study. *Comput. Mater. Sci.* **2017**, *128*, 287–293. [CrossRef]
24. Ramasubramaniam, A.; Naveh, D. Mn-doped monolayer MoS_2: An atomically thin dilute magnetic semiconductor. *Phys. Rev. B* **2013**, *87*, 195201. [CrossRef]
25. Wang, Y.; Li, S.; Yi, J. Electronic and magnetic properties of Co doped MoS_2 monolayer. *Sci. Rep.* **2016**, *6*, 24153. [CrossRef]
26. Deng, J.; Li, H.; Xiao, J.; Tu, Y.; Deng, D.; Yang, H.; Tian, H.; Li, J.; Ren, P.; Bao, X. Triggering the electrocatalytic hydrogen evolution activity of the inert two-dimensional MoS_2 surface via single-atom metal doping. *Energy Environ. Sci.* **2015**, *8*, 1594–1601. [CrossRef]
27. Chuang, S.; Battaglia, C.; Azcatl, A.; McDonnell, S.; Kang, J.S.; Yin, X.; Tosun, M.; Kapadia, R.; Fang, H.; Wallace, R.M.; et al. MoS_2 P-type transistors and diodes enabled by high work function MoOx contacts. *Nano Lett.* **2014**, *14*, 1337–1342. [CrossRef]
28. Fontana, M.; Deppe, T.; Boyd, A.K.; Rinzan, M.; Liu, A.Y.; Paranjape, M.; Barbara, P. Electron-hole transport and photovoltaic effect in gated MoS_2 Schottky junctions. *Sci. Rep.* **2013**, *3*, 1634. [CrossRef]
29. Ross, J.S.; Klement, P.; Jones, A.M.; Ghimire, N.J.; Yan, J.; Mandrus, D.G.; Taniguchi, T.; Watanabe, K.; Kitamura, K.; Yao, Y.; et al. Electrically tunable excitonic light-emitting diodes based on monolayer WSe2 p-n junctions. *Nat. Nanotechnol.* **2014**, *9*, 268–272. [CrossRef]
30. Zhang, Y.J.; Ye, J.T.; Yomogida, Y.; Takenobu, T.; Iwasa, Y. Formation of a stable p–n junction in a liquid-gated MoS_2 ambipolar transistor. *Nano Lett.* **2013**, *13*, 3023–3028. [CrossRef]
31. Mouri, S.; Miyauchi, Y.; Matsuda, K. Tunable photoluminescence of monolayer MoS_2 via chemical doping. *Nano Lett.* **2013**, *13*, 5944–5948. [CrossRef]
32. Lin, J.D.; Han, C.; Wang, F.; Wang, R.; Xiang, D.; Qin, S.; Zhang, X.-A.; Wang, L.; Zhang, H.; Wee, A.T.S.; et al. Electron-doping-enhanced trion formation in monolayer molybdenum disulfide functionalized with cesium carbonate. *ACS Nano* **2014**, *8*, 5323–5329. [CrossRef]
33. Tongay, S.; Zhou, J.; Ataca, C.; Liu, J.; Kang, J.S.; Matthews, T.S.; You, L.; Li, J.; Grossman, J.C.; Wu, J. Broad-range modulation of light emission in two-dimensional semiconductors by molecular physisorption gating. *Nano Lett.* **2013**, *13*, 2831–2836. [CrossRef]
34. Sasaki, S.; Kobayashi, Y.; Liu, Z.; Suenaga, K.; Maniwa, Y.; Miyauchi, Y.; Miyata, Y. Growth and optical properties of Nb-doped WS_2 monolayers. *Appl. Phys. Express* **2016**, *9*, 071201. [CrossRef]
35. Lin, D.Y.; Jheng, J.J.; Ko, T.S.; Hsu, H.P.; Lin, C.F. Doping with Nb enhances the photoresponsivity of WSe_2 thin sheets. *AIP Adv.* **2018**, *8*, 055011. [CrossRef]

36. Aspnes, D.E. *Handbook on Semiconductor*; Moss, T.S., Ed.; North-Holland: New York, NY, USA, 1996; Volume 2, p. 109. [CrossRef]
37. Aspnes, D.E.; Studna, A.A. Schottky-barrier electroreflectance: Application to GaAs. *Phys. Rev. B* **1973**, *7*, 4605–4625. [CrossRef]
38. Suh, J.; Tan, T.L.; Zhao, W.; Park, J.; Lin, D.Y.; Park, T.E.; Kim, J.; Jin, C.; Saigal, N.; Ghosh, S.; et al. Reconfiguring crystal and electronic structures of MoS_2 by substitutional doping. *Nat. Commun.* **2018**, *9*, 199. [CrossRef]
39. Zelewski, S.J.; Kudrawiec, R. Photoacoustic and modulated reflectance studies of indirect and direct band gap in van der Waals crystals. *Sci. Rep.* **2017**, *7*, 15365. [CrossRef]
40. Wang, T.; Andrews, K.; Bowman, A.; Hong, T.; Koehler, M.; Yan, J.; Mandrus, D.; Zhou, Z.; Xu, Y.Q. High performance WSe_2 phototransistors with 2D/2D ohmic contacts. *Nano Lett.* **2018**, *18*, 2766–2771. [CrossRef]
41. Dhyani, V.; Das, S. High-speed scalable silicon-MoS_2 p-n heterojunction photodetectors. *Sci. Rep.* **2017**, *7*, 44243. [CrossRef]
42. Di Bartolomeo, A.; Genovese, L.; Foller, T.; Giubileo, F.; Luongo, G.; Croin, L.; Liang, S.J.; Ang, L.K.; Schleberger, M. Electrical transport and persistent photoconductivity in monolayer MoS_2 phototransistors. *Nanotechnology* **2017**, *28*, 214002. [CrossRef]
43. Ko, T.S.; Huang, C.C.; Lin, D.Y.; Ruan, Y.J.; Huang, Y.S. Electrical and optical properties of Co-doped and undoped MoS_2. *Jpn. J. Appl. Phys.* **2016**, *55*, 04EP06. [CrossRef]
44. Wu, D.; Jiang, Y.; Li, S.; Li, F.; Li, J.; Lan, X.; Zhang, Y.; Wu, C.; Luo, L.; Jie, J. Construction of high-quality CdS:Ga nanoribbon/silicon heterojunctions and their nano-optoelectronic applications. *Nanotechnology* **2011**, *22*, 405201. [CrossRef]
45. Lou, Z.; Zeng, L.; Wang, Y.; Wu, D.; Xu, T.; Shi, Z.; Tian, Y.; Li, X.; Tsang, Y.H. High-performance MoS_2/Si heterojunction broadband photodetectors from deep ultraviolet to near infrared. *Opt. Lett.* **2017**, *42*, 3335–3338. [CrossRef]
46. Zhang, Y.; Yu, Y.; Mi, L.; Wang, H.; Zhu, Z.; Wu, Q.; Zhang, Y.; Jiang, Y. In situ fabrication of vertical multilayered MoS_2/Si homotype heterojunction for high-speed visible–near-infrared photodetectors. *Small* **2016**, *12*, 1062–1071. [CrossRef]